npj Computational Materials

www.nature.com/npjcompumats

ARTICLE OPEN

Check for updates

Tuning two-dimensional electron and hole gases at $LaInO_3$/$BaSnO_3$ interfaces by polar distortions, termination, and thickness

Wahib Aggoune[1]✉ and Claudia Draxl[1]

Two-dimensional electron gases (2DEG), arising due to quantum confinement at interfaces between transparent conducting oxides, have received tremendous attention in view of electronic applications. Here, we explore the potential of interfaces formed by two lattice-matched wide-gap oxides of emerging interest, i.e., the polar, orthorhombic perovskite $LaInO_3$ and the nonpolar, cubic perovskite $BaSnO_3$, employing first-principles approaches. We find that the polar discontinuity at the interface is mainly compensated by electronic relaxation through charge transfer from the $LaInO_3$ to the $BaSnO_3$ side. This leads to the formation of a 2DEG hosted by the highly dispersive Sn-*s*-derived conduction band and a 2D hole gas of O-*p* character, strongly localized inside $LaInO_3$. We rationalize how polar distortions, termination, thickness, and dimensionality of the system (periodic or non-periodic) can be exploited in view of tailoring the 2DEG characteristics, and why this material is superior to the most studied prototype $LaAlO_3$/$SrTiO_3$.

npj Computational Materials (2021)7:174 ; https://doi.org/10.1038/s41524-021-00646-x

INTRODUCTION

Heterostructures of transparent conducting oxides (TCOs) have attracted the attention of researchers in view of both fundamental research as well as potential applications[1,2]. Among them, interfaces of the perovskite materials $LaAlO_3$ and $SrTiO_3$ are the most studied prototypes due to the emergence of fascinating physical phenomena including superconductivity, ferromagnetism[3], and interfacial two-dimensional electron gases (2DEG)[1]. The latter is mainly a consequence of the electronic reconstruction to compensate the interfacial polar discontinuity induced by the deposition of the polar material $LaAlO_3$ formed by alternatingly charged $(LaO)^+$ and $(AlO_2)^-$ planes on a neutral, TiO_2-terminated $SrTiO_3$ substrate. The 2DEG density confined within the $SrTiO_3$ side of the interface can reach 0.5 electrons (*e*) per a^2 (*a* being the lattice parameter of $SrTiO_3$), corresponding to $\sim 3.3 \times 10^{14}$ cm^{-2} for a complete compensation of the formal polarization induced within $LaAlO_3$[4]. However, in real samples, the presence of defects impacts both polar discontinuity and electronic reconstruction, and thus carrier mobilities[5]. This includes cation intermixing[5,6], oxygen vacancies[7], edge dislocations[8], and changes in surface stoichiometry[9]. Overall, the electron mobilities at such an interface are very sensitive to growth conditions[5]. Besides these extrinsic effects, the low interfacial mobility of this material system is also caused by the low-dispersion (large effective electron masses) of the partially occupied Ti-*d* states. Further, scattering of electrons within these bands induced by significant electron–phonon coupling (EPC) decreases the mobility from 10^4 cm^2 V^{-1} s^{-1} at low temperature, to 1 cm^2 V^{-1} s^{-1} at room temperature[1,10].

According to the polar-catastrophe model, in a perfect $LaAlO_3$/$SrTiO_3$ interface, the formal polarization (P^0_{LAO}) allows for an insulator-to-metal transition at the interface beyond a certain thickness (t_c) of $LaAlO_3$. Estimating this quantity by considering the energy difference between the valence-band edge of $LaAlO_3$ and the conduction-band edge of $SrTiO_3$[4,11], one obtains a value of 3.5 unit cells. Higher t_c values reported theoretically and experimentally are due to structural relaxations, i.e., polar distortions that induce a polarization opposite to P^0_{LAO}. Such polar distortions that are not considered in the polar-catastrophe model maintain the insulating character of the interface above 3.5 unit cells as confirmed theoretically[12,13] and later observed experimentally[14]. These distortions appear mainly in the $LaAlO_3$ side of the interface and arise due to changes in inter-plane distances between La and Al planes upon interface formation. More recently, a competition between polar and nonpolar distortions through octahedra tilts has been observed[15]. Interestingly, the dependence of the octahdra tilts on the $LaAlO_3$ thickness can be exploited to tune the functionality of such interface[15]. We expect fascinating characteristics to occur when involving a polar material with pristine octahedral distortions, such as a perovskite with an orthorhombic primitive cell.

Focusing first on nonpolar candidates as the substrate, cubic $BaSnO_3$ (BSO) has emerged as a most attractive system to overcome the limitations of $SrTiO_3$, as it exhibits extraordinary room-temperature mobilities, reaching 320 cm^2 V^{-1} s^{-1}[16–21]. This value is the highest ever measured in a TCO and attributed to the low effective electron mass, as well as to the long relaxation time of the longitudinal optical phonon scattering compared to $SrTiO_3$[16,22,23]. In contrast to other suggested polar materials to be combined with $BaSnO_3$, such as $LaScO_3$[17], $LaGaO_3$[18], or $LaAlO_3$[24], $LaInO_3$ (LIO) has the advantage of being nearly lattice-matched to $BaSnO_3$ and exhibiting a favorable band offset to confine a 2DEG within the $BaSnO_3$ side[19–21,25,26]. Interestingly, it has an orthorhombic structure with tilted InO_6 octahedra, thus is ideal for exploring also the interfaces made of tilted and nontilted components.

In a previous work[27], it was shown by transmission electron microscopy (TEM) that $LaInO_3$ can be coherently grown on (001) $BaSnO_3$, forming a sharp interface with negligible atomic disorder or misfit dislocations. This characteristic makes such an interface fascinating, since—as reported for $LaAlO_3$/$SrTiO_3$[8]—the interface conductivity and the mobility of the electron gas are enhanced by minimizing the dislocation density. Later it was shown by HRTEM

[1]Institut für Physik and IRIS Adlershof, Humboldt-Universität zu Berlin, 12489 Berlin, Germany. ✉email: aggoune@physik.hu-berlin.de

analysis[28] that even if the BaO termination of the (001) $BaSnO_3$ surface is most favorable, the $LaInO_3/BaSnO_3$ interface (termed LIO/BSO from now on) is characterized by the LaO/SnO_2 termination, which is key for the formation of a 2DEG. Thereby, cation intermixing at the interface was rated to be negligible. Therefore, the combination of $LaInO_3$ and $BaSnO_3$ exhibits all the key features and appears superior to $LaAlO_3/SrTiO_3$ interfaces for reaching a high mobility 2DEG.

In this work, we explore the characteristics of ideal LIO/BSO interfaces, based on density functional theory (DFT), also employing many-body perturbation theory where needed. We focus only on intrinsic effects that may play a role in compensating the interfacial polar discontinuity, i.e., electronic reconstruction (formation of 2DEG) and possible structural distortions (formation of a depolarization field). Considering first periodic heterostructures, we address the competition between the polar distortions and the 2DEG charge density to compensate the interfacial polar discontinuity, upon increasing the thickness of the polar $LaInO_3$ block. Second, we discuss the impact of the interface termination that may give rise to either a 2DEG or a 2D hole gas (2DHG). Finally, motivated by the advancements in synthesis techniques and in control of nanoscale structures[29], we provide a detailed comparison between the characteristics of the 2DEG in a periodic heterostructure and a non-periodic LIO/BSO interface, discussing how one can exploit dimensionality for tailoring the properties of the 2DEG. Overall, our results demonstrate the potential of this material combination for tuning and achieving high electron density and mobility.

RESULTS AND DISCUSSION

Pristine materials

Before discussing the results for the periodic heterostructures LIO/BSO, we summarize the basic properties of the pristine materials. $BaSnO_3$ crystallizes in the cubic space group $Pm\bar{3}m$ and is built by alternating neutral $(BaO)^0$ and $(SnO_2)^0$ planes along the Cartesian directions, making it a nonpolar material. Its static dielectric constant was estimated to be about 20[16]. The calculated lattice constant of 4.119 Å obtained with the PBEsol functional is in excellent agreement with experiment[16]. $LaInO_3$ has an orthorhombic perovskite structure of space group Pbnm, containing four formula units per unit cell. The optimized structural parameters $a = 5.70$ Å, $b = 5.94$ Å, and $c = 8.21$ Å are in good agreement with experimental values[30]. The corresponding pseudocubic unit cell is defined as to have the same volume per $LaInO_3$ formula as the orthorhombic structure (for more details, see Supplemental Information). Its calculated lattice parameter is about 4.116 Å. In $LaInO_3$, the InO_6 octahedra are tilted along the pseudocubic unit cell directions with an $a^-a^-c^+$ pattern according to the Glazer notation[31]. Considering the formal ionic charges of La (+3), In (+3), and O (−2), the charged $(LaO)^{+1}$ and $(InO_2)^{-1}$ planes along the pseudocubic unit cell [100], [010], and [001] directions make $LaInO_3$ a polar material (see Supplementary Fig. 1).

The calculated lattice mismatch between the cubic $BaSnO_3$ and the pseudocubic $LaInO_3$ unit cells is about 0.07%, suggesting a coherent interface as confirmed experimentally[27]. In the latter work, it was shown that $LaInO_3$ can be favorably grown on top of a (001) $BaSnO_3$ substrate along the three pseudocubic unit cell directions, preserving the polar discontinuity at the interface, regardless of the orientation. Here, we consider the interface formed by [001]-oriented $LaInO_3$ (i.e., $c = 8.21$ Å corresponds to the out-of-plane direction) on top of the (001) $BaSnO_3$ surface (see Supplementary Fig. 1).

The electronic properties of both bulk $BaSnO_3$ and $LaInO_3$ have been reported by us in previous works[32,33], revealing PBEsol band gaps of 0.9 and 2.87 eV, and quasiparticle band gaps of 3.5 and 5.0 eV, respectively, as obtained by the G_0W_0 correction to the results obtained by the exchange-correlation functional HSE06 (G_0W_0@HSE06). In both cases, the valence-band maximum is dominated by O-*p* states, while, the conduction-band minimum has Sn-*s* and In-*s* character, respectively.

Stoichiometric periodic heterostructures

In Fig. 1 we show a comprehensive compilation of the electronic properties of the LIO/BSO interface in a periodic heterostructure. Thereby, n-type (LaO/SnO_2) and p-type (InO_2/BaO) building blocks are periodically replicated in the out-of-plane direction (*z*). In this case, the system is stoichiometric and ideally suited for investigating the electronic reconstruction due to the polar discontinuity. The $BaSnO_3$ block has a thickness of 10 unit cells which is enough to minimize the interaction with its replica. It is determined by making sure that the central part of the $BaSnO_3$ block behaves like its bulk counterpart (see Supplementary Fig. 2). The $LaInO_3$ block has a thickness of 12 pseudocubic unit cells. (We use the notation LIO_{12}/BSO_{10} heterostructure in the following). Since the $LaInO_3$ block has different terminations on the two sides, a formal polarization of $P_0 = e/2a^2 = 0.47$ C m^{-2}, oriented from the $(InO_2)^{-1}$ to the $(LaO)^{+1}$ plane, is induced (black arrow in the bottom panel of Fig. 1). As $BaSnO_3$ is a nonpolar material, this gives rise to a polar discontinuity at the interface.

The charge reconstruction is evident from the electronic band structure (Fig. 1e) showing that the combination of these two insulators has metallic character. From the local density of states (LDOS, per unit cell) depicted in Fig. 1a, along the *z* direction, we can clearly see that the dipole induced within the $LaInO_3$ side causes an upward shift of the valence-band edge, evolving between the $(LaO)^{+1}$ and $(InO_2)^{-1}$ terminations. This is also reflected in the in-plane averaged electrostatic potential shown in Fig. 1b (for more details see Supplementary Fig. 9). At the latter termination, the valence-band maximum crosses the Fermi level inside $LaInO_3$, leading to a charge transfer to the $BaSnO_3$ side in order to compensate the polar discontinuity. Consequently, the bottom of the conduction band of $BaSnO_3$ becomes partially occupied, giving rise to a 2DEG confined within three unit cells (~10 Å). A 2DHG forms in the $LaInO_3$ side localized within one pseudocubic unit cell (~4 Å). Integrating over these now partially occupied conduction states (see Supplementary methods), we find that the 2DEG density reaches a value of 2.7×10^{14} cm^{-2}, i.e., ~0.46 *e* per a^2 (a^2 being the unit cell area of bulk $BaSnO_3$). Obviously, the same value is obtained for the 2DHG when integrating over the now empty parts of the valence bands. The charge distribution shown in Fig. 1d reveals that the 2DEG is located mainly within the SnO_2 plane and exhibits Sn-*s* character. This highly dispersive *s*-band suggests high mobility, unlike the situation in $LaAlO_3/SrTiO_3$. These results demonstrate the exciting potential of such a material combination as an ideal platform for achieving a high-density 2DEG. We also highlight the importance of the well-confined 2DHG hosted by O-*p* states in view of p-type conductivity. We note that in $SrTiO_3/LaAlO_3/SrTiO_3$, another heterostructure[34] formed by a polar and a nonpolar material, only recently the presence of a 2DHG has been confirmed experimentally[29]. The coexistence of high-density well-confined electron and hole gases within one system as shown here, appears as a promising platform for exploring intriguing phenomena such as long-lifetime bilayer excitons[35] or Bose–Einstein condensation[36].

Polar distortions in stoichiometric periodic heterostructures

The 2DEG density reached in the periodic heterostructure LIO_{12}/BSO_{10}, being slightly lower than 0.5 *e* per a^2, indicates that polar distortions are involved to partially compensate for the polar discontinuity. Looking into its optimized geometry, we find that the tilt of the octahedra decreases gradually from the $LaInO_3$ to the $BaSnO_3$ side (see Fig. 1, bottom panel). Consequently, the out-of-plane lattice spacing increases close to the interface by about 3% (see Supplementary Fig. 2), in good agreement with an experimental observation[26]. We also find that the out-of-plane

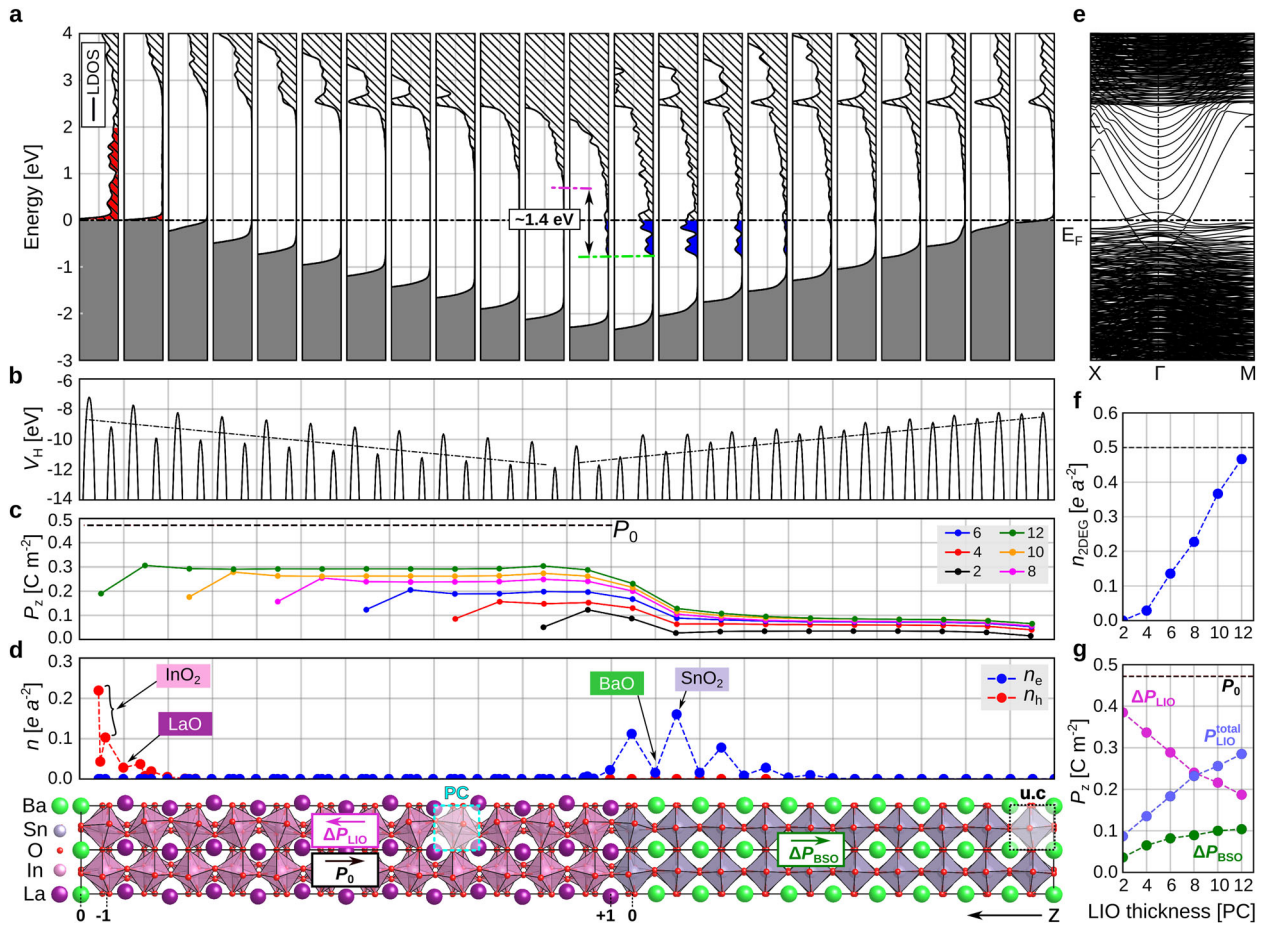

Fig. 1 Stoichiometric periodic heterostructure. The system is formed by LIO_{12}/BSO_{10} in out-of-plane direction z (bottom), which is shared between panels (a–d) as their horizontal axis. P_0 is the formal polarization oriented from the $(InO_2)^{-1}$ to the $(LaO)^{+1}$ plane. **a** Local density of states per unit cell (LDOS) where the Fermi level is set to zero (also in panel (**e**)). The shaded gray area indicates the occupied valence band. The partially unoccupied valence (hole) and the occupied conduction (electron) states, resulting from electronic reconstruction, are highlighted by red and blue color, respectively. The dashed green and pink lines indicate the alignment of the conduction-band edges of $BaSnO_3$ and $LaInO_3$ at the interface. **b** In-plane averaged electrostatic potential along the *z* direction. The dashed lines are guides to the eye, highlighting the trend of the potential. **c** Total polarization per unit cell computed for different $LaInO_3$ thicknesses (in units of the pseudocubic unit cell, PC). **d** Distribution of the electron (hole) charge densities obtained by integrating over the occupied conduction (unoccupied valence) states shown with blue (red) colored area in panel (**a**). **e** Electronic band structure along X-Γ-M. **f** Density of the 2DEG in electrons per $BaSnO_3$ surface unit cell (*e* per a^2). **g** Total polarization (P^{LIO}_{total}, violet) within the $LaInO_3$ block and changes of polar distortions within the $LaInO_3$ (ΔP_{LIO}, magenta) and $BaSnO_3$ (ΔP_{BSO}, green) side as a function of the $LaInO_3$ thickness. The respective orientations are shown in the structural model.

displacements of the inequivalent O atoms are not the same within all octahedra (see Supplementary Figs. 2 and 3). Moreover, the distances between AO and BO_2 planes (A = Ba, La and B = Sn, In) across the interface are also unequal (see Supplementary Fig. 2). Using a simple linear approximation for the local polarization based on Born effective charges (Z^*)[37,38] of the atomic species (calculated for the pristine materials), we obtain a qualitative trend of the out-of-plane polarization induced by such structural distortions (see Supplementary discussion). We note that due to the tilt of the octahedra, calculating the polarization for such a heterostructure is less straightforward than for, e.g., $LaAlO_3/SrTiO_3$. We find that the structural distortions within the $LaInO_3$ side induce a polarization ΔP_{LIO} that counteracts the formal polarization P_0. Moreover, the polar discontinuity at the interface is reduced by structural distortions within the $BaSnO_3$ side, inducing ΔP_{BSO} that is parallel to P_0. The total polarization within the $LaInO_3$ side, P^{LIO}_{total}, shown in Fig. 1g is the sum of $-\Delta P_{LIO}$ and P_0. As expected for the particular case of LIO_{12}/BSO_{10}, the average polarization within $LaInO_3$ (P^{LIO}_{total}) is smaller than P_0 due to partial compensation by structural distortions. For this reason, the 2DEG density mentioned above is smaller than 0.5 *e* per a^2. For better grasping of the polar discontinuity at the interface, we plot the total polarization along the *z* direction (see Fig. 1c). Focusing first on the particular case of LIO_{12}/BSO_{10}, we can clearly see that within the $LaInO_3$ side, it is smaller than P_0 and also non-negligible inside $BaSnO_3$, making the polar discontinuity at the interface less pronounced. As we provide only a qualitative analysis of the polarization, we do not expect a full match between the values of the 2DEG and the corresponding polarization discontinuity. However, the obtained trend of the polarization strength is valuable to understand and explain the relationship between the calculated 2DEG density and the $LaInO_3$ thickness.

Impact of the $LaInO_3$ thickness in stoichiometric periodic heterostructures

Now, we fix the thickness of the $BaSnO_3$ building block to 10 unit cells and vary that of $LaInO_3$ between 2 and 12 pseudocubic unit cells, labeling the systems LIO_m/BSO_{10} ($m = 2, 4, 6, 8, 10, 12$). Before discussing the results, we note that the critical thickness, t_c, for an insulator-to-metal transition at the interface is about one

pseudocubic $LaInO_3$ unit cell, when ignoring effects from structural relaxation as given by the polar-catastrophe model[4,11]. This value is obtained as $t_c = \epsilon_0\epsilon_{LIO}\Delta E/eP^0_{LIO}$. Here, $\epsilon_{LIO} \sim 24$ is the relative static dielectric constant of $LaInO_3$[30,39], and $\Delta E = 1$ eV represents the energy difference between the valence-band edge of $LaInO_3$ and the conduction-band edge of $BaSnO_3$ at the interface, obtained by the PBEsol functional (see Fig. 1a). In contrast to the unrelaxed LIO_2/BSO_{10} system, where we find metallic character, with full electronic reconstruction of 0.5 *e* per a^2 (see Supplementary Fig. 4), atomic relaxations lead to semiconducting character, i.e., no formation of 2DEG (see Fig. 1f). We observe that the polar distortions that counteract the formal polarization P_0, hamper the electronic reconstruction at the interface and, thus, the formation of a 2DEG, up to a critical thickness of 4 pseudocubic $LaInO_3$ unit cells (see Fig. 1f). This result highlights the importance of structural relaxations for compensating the polar discontinuity and stabilizing the interface.

Focusing on the electronic charge, we find that at a thickness of 4 pseudocubic $LaInO_3$ unit cells, the density of the 2DEG is only about 0.03 *e* per a^2 (see Fig. 1f), i.e., distinctively smaller than the nominal value of 0.5 *e* per a^2. On increasing the $LaInO_3$ thickness, the 2DEG density increases progressively and reaches a value of ~0.46 *e* per a^2 with 12 pseudocubic $LaInO_3$ unit cells. This means that the polar distortions are also non-negligible beyond the critical thickness. In Fig. 1g, we display the averages of ΔP_{LIO} and ΔP_{total} for the considered structures LIO_m/BSO_{10}, finding that the polar distortions (total polarization) is maximal (minimal) at two pseudocubic $LaInO_3$ unit cells and decreases (increases) with $LaInO_3$ thickness. ΔP_{BSO} increases with $LaInO_3$ thickness, but it is smaller than its counterpart in $LaInO_3$. As a result, the polar discontinuity at the interface increases with increasing $LaInO_3$ thickness (see Fig. 1c). Hence, the 2DEG density increases accordingly in order to compensate it (see Fig. 1f).

For a more reliable estimation of the critical thickness of $LaInO_3$ for an insulator-to-metal transition, we evaluate ΔE by considering the quasiparticle band gaps of the constituents[32,33]. Applying a scissor shift to the PBEsol band offset leads to a quasiparticle value of $\Delta E = 3.4$ eV, in agreement with the band offset reported in ref. [20] (see Supplementary discussion). Thus, we obtain a $t_c = 4$ pseudocubic $LaInO_3$ unit cell which is increased by 3 pseudocubic unit cells compared to that given by PBEsol offset (one pseudocubic unit cell). For the relaxed structures, we estimate t_c to be about seven pseudocubic $LaInO_3$ unit cells when considering quasiparticle band gaps, which is distinctively larger than the 4 pseudocubic unit cells derived from PBEsol (see Fig. 1f). This result indicates that a thick $LaInO_3$ component is needed to reach high 2DEG densities in periodic heterostructures, as both sides contribute to the compensation of the polar discontinuity through atomic distortions. This result is in line with a previous theoretical discussion reported for oxide interfaces[13].

Proceeding now to the nature of the atomic distortions, we find that, in contrast to the $LaAlO_3/SrTiO_3$ interface where the unequal distances between La and Al planes dominate[14], the unequal displacements of the inequivalent oxygen atoms are most decisive for the polar distortions in the $LaInO_3$ side of the interface (see Supplementary Fig. 2). This behavior is governed by the gradual tilts of octahedra across the interface which facilitates the compensation of the polar discontinuity. This indicates that below the critical thickness this compensation happens through such atomic distortions, rather than elimination by ionic intermixing or other defects, explaining the sharp interface and negligible intermixing observed experimentally[27]. The latter characteristic is crucial for achieving a high-density 2DEG beyond t_c. The band offset at the interface shows that the conduction-band minimum of $BaSnO_3$ is about 1.4 eV below that of $LaInO_3$, confining the 2DEG at the $BaSnO_3$ side (see Fig. 1a).

Non-stoichiometric nn-type periodic heterostructure

By adopting thicker polar building blocks, i.e., above 12 pseudocubic unit cells, the interaction between the n-type and the p-type interfaces is prevented. Due to the considerable computational costs, several models were proposed to predict the characteristics of such situations in oxide interfaces[13]. One of them is to consider non-stoichiometric structures, where the polar $LaInO_3$ block is terminated by a $(LaO)^{+1}$ plane on both sides. In this case, termed nn-type periodic heterostructure, the system is self-doped as the additional $(LaO)^{+1}$ layer serves as a donor. As the $LaInO_3$ building block is symmetric, the formal polarization P_0 is induced from the middle of the slab outwards on both sides, which compensate each other. In this way, the built-in potential inside the $LaInO_3$ is avoided, while the discontinuity at the LIO/BSO interface is preserved. To this end, we consider a periodic heterostructure formed by 10 $BaSnO_3$ unit cells and 10 pseudocubic $LaInO_3$ unit cells, which is large enough to minimize the interaction between the periodic n-type interfaces (see Fig. 2 (bottom) and Supplementary Fig. 6).

The electronic band structure, obtained by PBEsol, shows that this system has metallic character, where the partial occupation of the conduction band amounts to 1 *e* per a^2 (see Fig. 2e). The corresponding effective electron mass, being 0.24 m_e, is quite low compared with that of $LaAlO_3/SrTiO_3$ interfaces (0.38 m_e[34]), and suggests a high electron mobility. This value is close to that found for pristine $BaSnO_3$ (0.17 m_e obtained by PBEsol, 0.2 m_e by G_0W_0)[32]. In pristine $SrTiO_3$, a transition from band-like conduction (scattering of renormalized quasiparticles) to a regime governed by incoherent contributions due to the interaction between the electrons and their phonon cloud has been reported upon increasing temperature[40]. In $BaSnO_3$, the relaxation time for the longitudinal optical phonon scattering is found to be larger compared to $SrTiO_3$, contributing to the high room-temperature mobility reported for the La-doped $BaSnO_3$ single crystals[23]. Based on this, a high room-temperature mobility is also expected at the here-investigated interfaces as this material combination basically preserves the structure of the pristine $BaSnO_3$[41]. Overall, significant polaronic effects are not expected. In both constituents, we find typical EPC effects on the electronic properties[32,33], i.e., a moderate renormalization of the band gap by zero point vibrations and temperature. Given the excellent agreement between theory and experiment that can explain all the features of the optical spectra[32,33], we conclude that polaronic distortions do not play a significant role. Thus, we do not expect a dramatically different behavior at the interfaces.

Before analyzing the spatial charge distribution, we note that in a pristine symmetric $LaInO_3$ slab, the electronic charge accumulates on its surfaces, accompanied by structural distortions that tend to screen the discontinuity of the polarization. Combined with $BaSnO_3$, the polar distortions vanish at the $LaInO_3$ side but appear in the $BaSnO_3$ building block and are accompanied by a charge redistribution (see Fig. 2a, c). In Fig. 2c, we display the polarization induced by the structural distortions along the slab. We find that the gradual decrease of the octahedra tilt from the $LaInO_3$ to the $BaSnO_3$ side enlarges the out-of-plane lattice spacing at the interface and enhances the unequal oxygen-cation displacements within the $BaSnO_3$ side (see Supplementary Fig. 6). This, in turn, induces a gradually decreasing polarization (ΔP_{BSO}) oriented away from the interface. Due to this local dipole, the $BaSnO_3$ conduction-band edge is shifted downwards near the interface, leading to partial charge redistribution (see Fig. 2a, d), and being also evident in the in-plane averaged electrostatic potential (Fig. 2b). Integrating the LDOS over the partially occupied conduction states, we find that the 2DEG is confined within three unit cells, amounting to 0.5 *e* per a^2 at each side (see Fig. 2d). Thereby the 2DEG is mainly hosted by Sn-*s* states within the SnO_2 planes. The valence and conduction-band edges at the $LaInO_3$ side are almost the same in all pseudocubic unit cells as

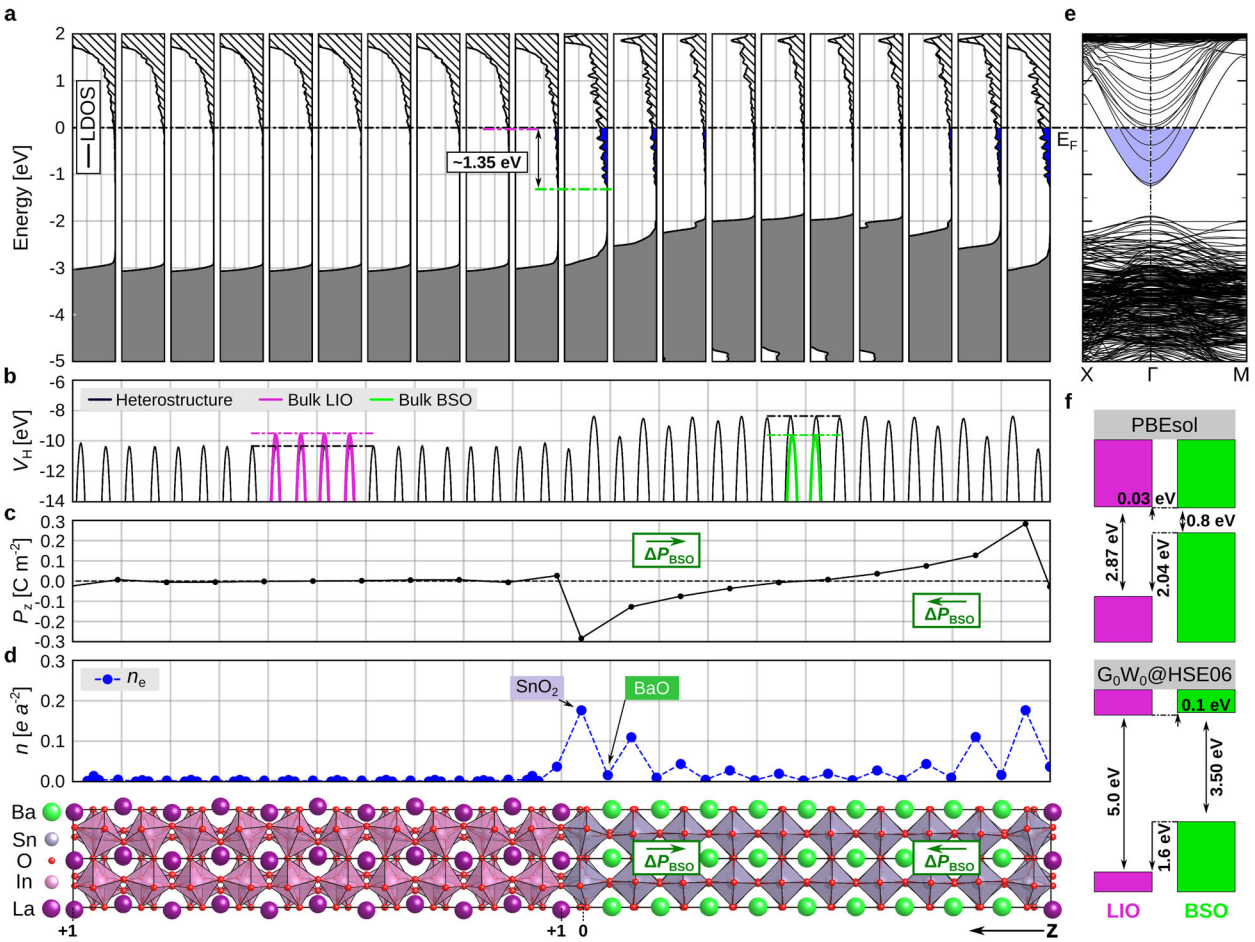

Fig. 2 Non-stoichiometric periodic nn-type heterostructure. The system is formed by LIO_{10}/BSO_{10} in out-of-plane direction z (bottom), which is shared between panels (**a**–**d**) as their horizontal axis. The $LaInO_3$ block is terminated by a $(LaO)^{+1}$ plane on both sides. **a** Local density of states per unit cell (LDOS). The Fermi level is set to zero, and the electron population of the (original) conduction bands is shown as shaded blue area (also in panel (**e**)). The dashed green and pink lines indicate the alignment of the conduction-band edges of the two materials at the interface. **b** In-plane averaged electrostatic potential along the *z* direction. **c** Total polarization per unit cell. **d** Distribution of the electron charge density obtained by integrating over the occupied conduction states indicated by the blue area in panel (**a**). **e** Electronic band structure along X-Γ-M. **f** Band alignment as obtained by using the band gaps of the bulk systems (PBEsol, top and G_0W_0@HSE06, bottom), considering the energy difference between the potential of the bulk and the periodic heterostructure as shown in panel (**b**). The alignment at the interface obtained by PBEsol can be seen in panel (**a**).

the polar distortions are negligible (only nonpolar tilts) (see Fig. 2a, c). These results are in line with the trend of the polarization and the 2DEG density obtained for the stoichiometric periodic system. While in the latter, we observed decreasing (increasing) structural distortions in the $LaInO_3$ ($BaSnO_3$) side as a function of $LaInO_3$ thickness (see Fig. 1g), here the polar distortions vanish (are enhanced) at the $LaInO_3$ ($BaSnO_3$) side of the interface. Consequently, the conduction-band minimum of the $BaSnO_3$ side is lowered by about 1.35 eV with respect to that of $LaInO_3$ (see Fig. 2a). This value is also in line with that estimated for the stoichiometric periodic heterostructure LIO_{12}/BSO_{10} (~1.4 eV). Such an offset is crucial for confining the 2DEG in order to reach a value of 0.5 *e* per a^2 (see Fig. 2a, d).

Note that here we can determine the band offsets by considering the respective quasiparticle gaps of the pristine materials[32,33], as well as an alternative approach based on the electrostatic potential[42] (see Fig. 2b and Supplementary discussion). We find that the conduction-band offset between the middle of the $BaSnO_3$ and $LaInO_3$ blocks is almost the same when using quasiparticle or PBEsol band gaps (see Fig. 2b, f). Thus, we conclude that PBEsol is good enough to capture band offset and charge distribution at the interface. The latter conclusions are confirmed by calculations using HSE06 for a smaller (feasible) nn-type system (see Supplementary discussion).

Non-stoichiometric pp-type periodic heterostructure

Calculations for a periodic pp-type heterostructure (see Supplementary Fig. 5) with $(InO_2)^{-1}$ termination on both sides of $LaInO_3$ reveal a 2DHG with a density of 0.5 *e* per a^2. Interestingly, the hole stays at the $LaInO_3$ side, confined within one pseudocubic unit cell. Like in the periodic nn-type heterostructure, the tilt of the octahedra decreases gradually from the $LaInO_3$ to the $BaSnO_3$ side. However, the BaO termination in the pp-type case favors nonpolar distortions within the $BaSnO_3$ side, i.e., equal displacements of the inequivalent O atoms, while polar distortions appear only in the $LaInO_3$ side. Consequently, local dipoles are induced in the latter, pushing up its valence-band edge above that of $BaSnO_3$ (see Supplementary Fig. 5). Hence, the 2DHG exhibiting O-*p* character stays on the $LaInO_3$ side of the interface. It has been shown recently by a combined theoretical and experimental investigation[28] that the n-type interface is more favorable than the p-type interface. Since, at the BaO-terminated p-type interface, the 2DHG stays within the $LaInO_3$ side, it contributes less to the compensation of the interfacial polar discontinuity. In contrast, the SnO_2-terminated n-type interface

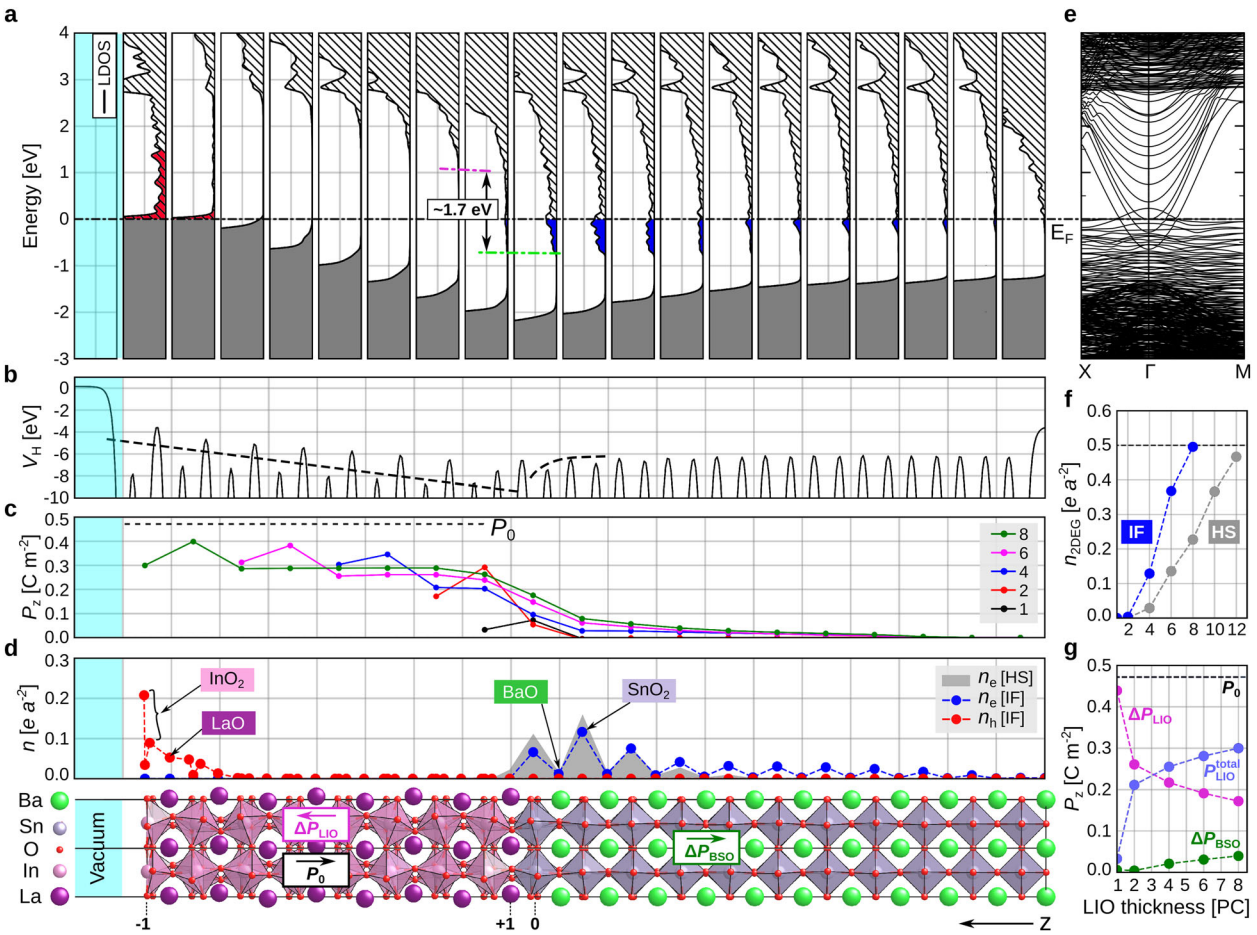

Fig. 3 Stoichiometric non-periodic interface (here termed IF). The system is formed by LIO_8/BSO_{11} in out-of-plane direction z (bottom), which is shared between panels (a–d) as their horizontal axis. P_0 is the formal polarization oriented from the $(InO_2)^{-1}$ plane towards the $(LaO)^{+1}$ plane at the interface. **a** Local density of states per unit cell (LDOS) with the Fermi level being set to zero (also in panel (**e**)). The shaded gray area indicates the occupied valence states. The depleted valence-band region (holes) and the occupied conduction-band region (electrons) resulting from electronic reconstruction, are highlighted by red and blue color, respectively. The dashed green and pink lines indicate the alignment of the conduction-band edges of the two materials at the interface. **b** In-plane averaged electrostatic potential along the *z* direction. **c** Total polarization per unit cell computed for different $LaInO_3$ thicknesses (in units of the pseudocubic unit cell, PC). **d** Distribution of the electron (hole) charge densities obtained by integrating the LDOS indicated by blue (red) color in panel (**a**). For comparison, the 2DEG distribution in the periodic heterostructure LIO_{12}/BSO_{10} (here termed HS) is shown by the shaded gray area. **e** Electronic band structure along X-Γ-M. **f** Density of the 2DEG in *e* per a^2 in the non-periodic (blue) and periodic (gray) heterostructures. **g** Total polarization (P^{LIO}_{total}, violet) within the $LaInO_3$ side and changes of polar distortions within $LaInO_3$ (ΔP_{LIO}, magenta) and $BaSnO_3$ (ΔP_{BSO}, green) side as a function of $LaInO_3$ thickness. The respective orientations are shown in the structural model.

allows for electronic charge transfer to the $BaSnO_3$ side, forming a 2DEG that compensates the interfacial polar discontinuity more efficiently (see Supplementary discussion).

Stoichiometric non-periodic interface

Now, we investigate the case of a non-periodic LIO/BSO interface, consisting of a thin $LaInO_3$ layer on top of a (001) $BaSnO_3$ substrate. Considering stoichiometric systems, we only focus on the n-type interface as it is predicted to be more favorable[28]. For $BaSnO_3$, we find that 11 unit cells are enough to capture the extension of the structural deformations and the 2DEG distribution away from the interface. We then vary the thickness of $LaInO_3$ between one and eight pseudocubic unit cells, labeling the systems as LIO_n/BSO_{11} ($n = 1$, 2, 4, 6, 8). In Fig. 3 (bottom panel), we show the optimized geometry of LIO_8/BSO_{11}. The $BaSnO_3$ substrate terminates with a $(SnO_2)^0$ plane at the interface, and the surface termination of $LaInO_3$ is a $(InO_2)^{-1}$ plane. Thus, $LaInO_3$ is stoichiometric and has a formal polarization of $P_0 = 0.47\ C\ m^{-2}$, oriented from the surface to the interface, as in the stoichiometric periodic heterostructures discussed above.

Electronic reconstruction, which leads to a metallic character, is evident from the resulting band structure, where the valence and conduction bands overlap at the Γ point (see Fig. 3e). In the LDOS, we clearly see that the dipole induced within $LaInO_3$ causes an upward shift of the valence-band edge (most pronounced at the surface) which is also evident in the in-plane averaged electrostatic potential (see Fig. 3a, b). At the surface, the valence-band edge crosses the Fermi level, leading to a charge transfer across the interface that counteracts the polar discontinuity (see Fig. 3a). Consequently, the bottom of the conduction band becomes partially occupied within the $BaSnO_3$ side, giving rise to a 2DEG that is confined within five unit cells (~20 Å) (see Fig. 3d). The 2DHG formed at the surface is localized within one pseudocubic $LaInO_3$ unit cell (~4 Å). In this case, the conduction-band minimum of the $BaSnO_3$ building block is about 1.7 eV below that of $LaInO_3$ (Fig. 1a), in agreement with an experimental observation of 1.6 eV[20]. Integrating the LDOS over the region of these partially filled states, we find that the 2DEG density (and likewise the 2DHG density) reaches a value of $2.9 \times 10^{14}\ cm^{-2}$, i.e., ~ 0.49 *e* per a^2.

By increasing the $LaInO_3$ thickness from one to eight pseudocubic unit cells, the polar distortions (ΔP_{LIO}) decrease, being accompanied by an electronic charge transfer from the surface to the interface (see Fig. 3f, g). Compared to the periodic heterostructure (Fig. 1c), they are less pronounced at the $BaSnO_3$ side (Fig. 3c). This enhances the polar discontinuity (see Supplementary Fig. 8), and thus the 2DEG density that reaches a higher value than in the periodic systems with similar $LaInO_3$ thickness (see Fig. 3f). Focusing on the charge confinement, the conduction-band edge in the $BaSnO_3$ side is gradually shifted up when moving away from the interface as ΔP_{BSO} is less pronounced. This allows an extension of the 2DEG up to five unit cells (~20 Å) in the $BaSnO_3$ (substrate) compared to three unit cells in the periodic heterostructure case (see Fig. 3d). The enhanced polar discontinuity reduces the critical thickness to only two pseudocubic $LaInO_3$ unit cells compared to four found for the periodic heterostructure, when relying on PBEsol (see Fig. 3f). Based on the quasiparticle band gaps, however, we estimate t_c to be five pseudocubic $LaInO_3$ unit cells in the non-periodic system compared to seven in the periodic case. Overall tuning of the 2DEG charge density through the $LaInO_3$ thickness is possible, and remarkably, also the type of heterostructure (i.e., periodic or non-periodic) impacts its spatial distribution. Both aspects can be exploited to tune the characteristic of the 2DEG.

In view of realistic applications, it is worth considering the results presented here in the context of existing experimental research on LIO/BSO interfaces. A main challenge here is the quality of the $BaSnO_3$ substrate[43]. Previous experimental works[20,26] investigated a field effect transistor, formed by a $LaInO_3$ gate and a La-doped $BaSnO_3$ channel on a $SrTiO_3$ substrate. An enhancement of conductance with increasing $LaInO_3$ thickness was observed, but there was no indication of a critical thickness for an insulator-to-metal transition at the interface. A maximal 2DEG density of only 3×10^{13} (0.05 e per a^2) was reported for 4 pseudocubic $LaInO_3$ unit cells, and a decrease beyond it. We assign the differences to our predictions for non-periodic interfaces mainly to the high density of structural defects (e.g., dislocations) due to the large mismatch (~5%) between the channel and the substrate. The La doping, needed to compensate the acceptors induced by such dislocations, may cause an alleviation of the polar discontinuity at the interface and, hence, limit the 2DEG density. On the other hand, it makes the system metallic without a clear critical thickness. With the recent advances in achieving high-quality $BaSnO_3$ and $LaInO_3$ single crystals[30,33,43], as well as interfaces[27,28], our predictions open up a perspective for exploring interfacial charge densities in combinations of these materials in view of potential electronic applications.

Conclusions

In summary, we have presented the potential of combining nonpolar $BaSnO_3$ and polar $LaInO_3$ for reaching a high interfacial carrier density. Our calculations show that, depending on the interface termination, both electron and hole gases can be formed that compensate the polar discontinuity. The gradual decrease of octahedra tilts from the orthorhombic $LaInO_3$ to the cubic $BaSnO_3$ side increases the out-of-plane lattice spacing at the interface and governs the unequal oxygen-cation displacements within the octahedra. The latter distortions induce a depolarization field, counteracting the formal polarization in the $LaInO_3$ block and hampering electronic reconstruction, i.e., the formation of a 2DEG at the interface up to a critical $LaInO_3$ thickness of seven (five) pseudocubic unit cells for periodic (non-periodic) heterostructures. While the PBSEsol functional provides a good description of the interfacial charge-density distributions as well as the type of band offset, it fails to determine t_c reliably, as the knowledge of the quasiparticle gaps of the pristine materials is required. The polar distortions (polar discontinuity) decrease (increase) with $LaInO_3$ thickness, leading to a progressive charge transfer until reaching a 2DEG density of 0.5 e per surface unit cell. The electronic charge density is hosted by a highly dispersive Sn-s-derived conduction band, suggesting a high carrier mobility. Overall, the 2DEG charge density can be tuned through the $LaInO_3$ thickness. Interestingly, also the type of interface (i.e., periodic or non-periodic heterostructure) strongly impacts its density and spatial confinement. All these effects can be exploited in view of tailoring the characteristics of the 2DEG.

METHODS

Theory

Ground-state properties are calculated using DFT, within the generalized gradient approximation (GGA) in the PBEsol parameterization[44] for exchange-correlation effects. All calculations are performed using FHI-aims[45], an all-electron full-potential package, employing numerical atom-centered orbitals. For all atomic species, we use a tight setting with a *tier* 2 basis set for oxygen, *tier1* + *fg* for barium, *tier1* + *gpfd* for tin, *tier 1* + *hfdg* for lanthanum, and *tier 1* + *gpfhf* for indium. The convergence criteria are 10^{-6} electrons for the density, 10^{-6} eV for the total energy, 10^{-4} eV Å^{-1} for the forces, and 10^{-4} eV for the eigenvalues. Lattice constants and internal coordinates are optimized for all systems until the residual forces on each atom are less than 0.001 eV Å^{-1}. The sampling of the Brillouin zone is performed with an $8 \times 8 \times 8$ **k**-grid for bulk $BaSnO_3$ and a $6 \times 6 \times 4$ **k**-grid for bulk $LaInO_3$. These parameters ensure converged total energies and lattice constants of 8 meV per atom and 0.001 Å, respectively. The Born effective charges in pristine systems are computed using exciting code[46] (see supplementary discussion).

For the heterostructures, a $6 \times 6 \times 1$ **k**-grid is used. The in-plane lattice parameters are fixed to $\sqrt{2}a_{BSO}$ (a_{BSO} being the bulk $BaSnO_3$ lattice spacing) (see Supplementary Fig. 1). For the non-periodic systems, vacuum of about 150 Å is included and a dipole correction is applied in the [001] direction in order to prevent unphysical interactions between neighboring replica. In this case, we fix the first two $BaSnO_3$ unit cells to the bulk structure to simulate the bulk-like interior of the substrate, and relax the other internal coordinates. For computing the electronic properties, a $20 \times 20 \times 1$ **k**-grid is adopted for all systems. This parameter ensures converged densities of states and electron/hole charge densities up to 0.01 e per a^2. Atomic structures are visualized using the software package VESTA[47].

DATA AVAILABILITY

Input and output files can be downloaded free of charge from the NOMAD Repository[48] at the following link: https://doi.org/10.17172/NOMAD/2021.03.10-1.

Received: 11 March 2021; Accepted: 7 October 2021;
Published online: 27 October 2021

REFERENCES

1. Ohtomo, A. & Hwang, H. Y. A high-mobility electron gas at the $LaAlO_3/SrTiO_3$ heterointerface. *Nature* **427**, 423 (2004).
2. Mannhart, J. & Schlom, D. G. Oxide interfaces—an opportunity for electronics. *Science* **327**, 1607–1611 (2010).
3. Bert, J. A. et al. Direct imaging of the coexistence of ferromagnetism and superconductivity at the $LaAlO_3/SrTiO_3$ interface. *Nat. Phys.* **7**, 767 (2011).
4. Nakagawa, N., Hwang, H. Y. & Muller, D. A. Why some interfaces cannot be sharp. *Nat. Mater.* **5**, 204 (2006).
5. Huijben, M. et al. Structure–property relation of $SrTiO_3/LaAlO_3$ interfaces. *Adv. Mater.* **21**, 1665–1677 (2009).
6. Chambers, S. et al. Instability, intermixing and electronic structure at the epitaxial $LaAlO_3/SrTiO_3$(001) heterojunction. *Surf. Sci. Rep.* **65**, 317 – 352 (2010).
7. Thiel, S., Hammerl, G., Schmehl, A., Schneider, C. W. & Mannhart, J. Tunable quasi-two-dimensional electron gases in oxide heterostructures. *Science* **313**, 1942–1945 (2006).
8. Thiel, S. et al. Electron scattering at dislocations in $LaAlO_3/SrTiO_3$ interfaces. *Phys. Rev. Lett.* **102**, 046809 (2009).
9. Xie, Y., Bell, C., Hikita, Y., Harashima, S. & Hwang, H. Y. Enhancing electron mobility at the $LaAlO_3/SrTiO_3$ interface by surface control. *Adv. Mater.* **25**, 4735–4738 (2013).
10. Cancellieri, C. et al. Polaronic metal state at the $LaAlO_3/SrTiO_3$ interface. *Nat. Commun.* **7**, 10386 (2016).

11. Reinle-Schmitt, M. et al. Tunable conductivity threshold at polar oxide interfaces. *Nat. Commun.* **3**, 932 (2012).
12. Pentcheva, R. & Pickett, W. E. Avoiding the polarization catastrophe in $LaAlO_3$ overlayers on $SrTiO_3$(001) through polar distortion. *Phys. Rev. Lett.* **102**, 107602 (2009).
13. Stengel, M. First-principles modeling of electrostatically doped perovskite systems. *Phys. Rev. Lett.* **106**, 136803 (2011).
14. Cantoni, C. et al. Electron transfer and ionic displacements at the origin of the 2D electron gas at the LAO/STO interface: direct measurements with atomic-column spatial resolution. *Adv. Mater.* **24**, 3952–3957 (2012).
15. Gazquez, J. et al. Competition between polar and nonpolar lattice distortions in oxide quantum wells: new critical thickness at polar interfaces. *Phys. Rev. Lett.* **119**, 106102 (2017).
16. Kim, H. J. et al. High mobility in a stable transparent perovskite oxide. *Appl. Phys. Express* **5**, 061102 (2012).
17. Paudel, T. R. & Tsymbal, E. Y. Prediction of a mobile two-dimensional electron gas at the $LaScO_3/BaSnO_3$(001) interface. *Phys. Rev. B* **96**, 245423 (2017).
18. Wang, Y., Tang, W., Cheng, J., Nazir, S. & Yang, K. High-mobility two-dimensional electron gas in $SrGeO_3$- and $BaSnO_3$-based perovskite oxide heterostructures: an ab initio study. *Phys. Chem. Chem. Phys.* **18**, 31924–31929 (2016).
19. Krishnaswamy, K. et al. $BaSnO_3$ as a channel material in perovskite oxide heterostructures. *Appl. Phys. Lett.* **108**, 083501 (2016).
20. Kim, U. et al. All-perovskite transparent high mobility field effect using epitaxial $BaSnO_3$ and $LaInO_3$. *APL Mater.* **3**, 036101 (2015).
21. Lee, W.-J. et al. Transparent perovskite barium stannate with high electron mobility and thermal stability. *Annu. Rev. Mater. Res.* **47**, 391–423 (2017).
22. Niedermeier, C. A. et al. Electron effective mass and mobility limits in degenerate perovskite stannate $BaSnO_3$. *Phys. Rev. B* **95**, 161202 (2017).
23. Niedermeier, C. A., Kamiya, T. & Moram, M. A. Polaron coupling constants in $BaSnO_3$. Preprint at https://arxiv.org/pdf/1612.01343v1.pdf (2016).
24. Chambers, S. A., Kaspar, T. C., Prakash, A., Haugstad, G. & Jalan, B. Band alignment at epitaxial $BaSnO_3/SrTiO_3$(001) and $BaSnO_3/LaAlO_3$(001) heterojunctions. *Appl. Phys. Lett.* **108**, 152104 (2016).
25. Kim, Y., Kim, Y. M., Shin, J. & Char, K. $LaInO_3/BaSnO_3$ polar interface on MgO substrates. *APL Mater.* **6**, 096104 (2018).
26. Kim, Y. M. et al. Interface polarization model for a 2-dimensional electron gas at the $BaSnO_3/LaInO_3$ interface. *Sci. Rep.* **9**, 16202 (2019).
27. Zupancic, M. et al. Role of the interface in controlling the epitaxial relationship between orthorhombic $LaInO_3$ and cubic $BaSnO_3$. *Phys. Rev. Mater.* **4**, 123605 (2020).
28. Zupancic, M., Aggoune, W., Draxl, C. & Albrecht, M. Termination at the $BaSnO_3$ surface and $LaInO_3/BaSnO_3$ interface. In preparation (2021).
29. Lee, H. et al. Direct observation of a two-dimensional hole gas at oxide interfaces. *Nat. Mater.* **17**, 231 (2018).
30. Galazka, Z. et al. Melt growth and physical properties of bulk laino3 single crystals. *Phys. Status Solidi (a)* **218**, 2100016 (2021).
31. Glazer, A. M. The classification of tilted octahedra in perovskites. *Acta Crystallogr., Sect. B* **28**, 3384–3392 (1972).
32. Aggoune, W. et al. Electronic and optical properties of cubic $BaSnO_3$: a combined theoretical and experimental study. Preprint at https://arxiv.org/abs/2105.07817 (2021).
33. Aggoune, W. et al. Fingerprints of optical absorption in the perovskite $LaInO_3$: insight from many-body theory and experiment. *Phys. Rev. B* **103**, 115105 (2021).
34. Maznichenko, I. V., Ostanin, S., Ernst, A., Henk, J. & Mertig, I. Formation and tuning of 2D electron gas in perovskite heterostructures. *Phys. Status Solidi B* **257**, 1900540 (2020).
35. Millis, A. J. & Schlom, D. G. Electron–hole liquids in transition-metal oxide heterostructures. *Phys. Rev. B* **82**, 073101 (2010).
36. Eisenstein, J. & MacDonald, A. Bose–Einstein condensation of excitons in bilayer electron systems. *Nature* **432**, 691–694 (2004).
37. King-Smith, R. D. & Vanderbilt, D. Theory of polarization of crystalline solids. *Phys. Rev. B* **47**, 1651–1654 (1993).
38. Resta, R., Posternak, M. & Baldereschi, A. Towards a quantum theory of polarization in ferroelectrics: the case of $KNbO_3$. *Phys. Rev. Lett.* **70**, 1010–1013 (1993).
39. Jang, D. H. et al. Single crystal growth and optical properties of a transparent perovskite oxide $LaInO_3$. *J. Appl. Phys.* **121**, 125109 (2017).
40. Zhou, J.-J. & Bernardi, M. Predicting charge transport in the presence of polarons: the beyond-quasiparticle regime in $SrTiO_3$. *Phys. Rev. Res.* **1**, 033138 (2019).
41. Krishnaswamy, K., Himmetoglu, B., Kang, Y., Janotti, A. & Van de Walle, C. G. First-principles analysis of electron transport in $BaSnO_3$. *Phys. Rev. B* **95**, 205202 (2017).
42. Nabok, D., Höffling, B. & Draxl, C. Energy-level alignment at organic/inorganic interfaces from first principles: example of poly(para-phenylene)/rock-salt ZnO (100). *Chem. Mater.* **31**, 7143–7150 (2019).
43. Galazka, Z. et al. Melt growth and properties of bulk $BaSnO_3$ single crystals. *J. Phys. Condens. Matter* **29**, 075701 (2016).
44. Perdew, J. P. et al. Restoring the density-gradient expansion for exchange in solids and surfaces. *Phys. Rev. Lett.* **100**, 136406 (2008).
45. Blum, V. et al. Ab initio molecular simulations with numeric atom-centered orbitals. *Comput. Phys. Commun.* **180**, 2175 – 2196 (2009).
46. Gulans, A. et al. Exciting: a full-potential all-electron package implementing density-functional theory and many-body perturbation theory. *J. Phys. Condens. Matter* **26**, 363202 (2014).
47. Momma, K. & Izumi, F. *VESTA3* for three-dimensional visualization of crystal, volumetric and morphology data. *J. Appl. Cryst.* **44**, 1272–1276 (2011).
48. Draxl, C. & Scheffler, M. The nomad laboratory: from data sharing to artificial intelligence. *J. Phys. Mater.* **2**, 036001 (2019).

ACKNOWLEDGEMENTS

This work was supported by the project BaStet (Leibniz Senatsausschuss Wettbewerb, No. K74/2017) and was performed in the framework of GraFOx, a Leibniz Science Campus, partially funded by the Leibniz Association. Partial funding was received by the Max Planck Graduate Center for Quantum Materials. We acknowledge the North-German Supercomputing Alliance (HLRN) for providing HPC resources that have contributed to the research results reported in this paper (project bep00078). W.A. thanks Martin Albrecht, Martina Zupancic, and Toni Markurt (Leibniz-Institut für Kristallzüchtung, Berlin) Dmitrii Nabok, Le Fang, and Sebastian Tillack (Humboldt-Universität zu Berlin), as well as Kookrin Char (Seoul National University) for fruitful discussions.

AUTHOR CONTRIBUTIONS

W.A. performed the atomistic simulations and analyzed the data. Both authors discussed the results and wrote the paper.

FUNDING

Open Access funding enabled and organized by Projekt DEAL.

COMPETING INTERESTS

The authors declare no competing interests.

ADDITIONAL INFORMATION

Supplementary information The online version contains supplementary material available at https://doi.org/10.1038/s41524-021-00646-x.

Correspondence and requests for materials should be addressed to Wahib Aggoune.

Reprints and permission information is available at http://www.nature.com/reprints

Publisher's note Springer Nature remains neutral with regard to jurisdictional claims in published maps and institutional affiliations.